POLITECNICO DI TORINO
Repository ISTITUZIONALE

A Method for Battery Sizing in Parallel P4 Mild Hybrid Electric Vehicles

(Article begins on next page)

10 April 2024

A METHOD FOR BATTERY SIZING IN PARALLEL P4 MILD HYBRID ELECTRIC VEHICLES

ABSTRACT– This article deals with a sensitivity analysis concerning the influence that the capacity of the battery in a parallel hybrid powertrain has on the vehicle energy regeneration. The architecture under analysis is constituted by an internal combustion engine, which provides traction to the front axle's wheels and an electric motor powering the rear wheels. The energy management system is based on a simple torque split strategy that distributes the driver required torque between front and rear machines as a function of battery and electric motor functional limitations (state of charge, temperatures and maximum admissible currents). Together with the selected driving cycles, the central role played by the battery size in the overall vehicle recoverable energy is evaluated, while the influence of the powertrain limitations is highlighted accounting both for uncertain parameters (e. g. initial state of charge) and for tunable parameters (e. g. maximum electric traction vehicle speed). Therefore, a method of the sizing the battery of a P4 mild hybrid electric vehicle, which allows the maximization of the braking energy recovery, is developed.

1. INTRODUCTION

The recent and always more stringent regulations regarding passenger vehicles' pollutant emissions in atmosphere (e. g. CO_2, PMs, CO, HC, NO_x) [1, 2, 3, 4] in the last years are pushing the car manufacturers to introduce modifications on their vehicles with the goal of increasing their overall efficiency. Standing in the field of internal combustion engines (ICEs) driven vehicles, possible improvements regard the engine (e.g. advanced injection systems and methods, downsizing, after-treatment techniques) [4, 5, 6] or the chassis (body weight reduction through the use of innovative materials, tires rolling resistance reduction, aerodynamic drag reduction) [7, 8].

Hybrid electric vehicles (HEVs) are promising technologies that make use of more than one source of energy to provide traction to the wheels or allow part of the energy, that otherwise would be wasted in heat during the braking, to be recovered and stored for future use [2, 4, 9, 10].

Several hybrid vehicles architectures have been analyzed and tested both in simulation and in real-life scenarios, set into production. Based on the size of the electric powertrain HEVs can be classified as [2, 4]: 1) Micro Hybrids, owning the possibility of Start&Stop implementation 2) Mild Hybrids, offering regenerative braking and engine assist functions, 3) Full Hybrids, in which previous functions are merged together with the capability of pure electric traction, 4) Plug-in Hybrids (PHEV), for which the main peculiarity is the possibility to connect the electric battery to the electrical grid. Another interesting classification is based on the position of the secondary energy converter [2, 11, 12] as shown in Figure 1:

- P_{1f} (P_0). Belt driven Integrated Starter Generator installed on the front end accessory drive (FEAD);
- P_{1r} (P_1). The electric motor is positioned directly on the engine crankshaft, before the mechanical clutch;
- P_2. The electric motor is mounted downstream the mechanical clutch, hence the complete uncoupling between vehicle and ICE can be performed;
- $P_{2.5}$. The electric motor is integrated into the transmission;
- P_3. The electric motor is placed at the output of the secondary transmission shaft;
- P_4. The electric motor is placed on opposite axle with respect to the one in which the ICE is positioned.

Some of the aforementioned architectures require few changes to the overall vehicle structure while in some others the powertrain should be consistently modified. Therefore, in order to reduce the time to market and gain short terms benefits, manufacturers tend to avoid the complete powertrain and car body re-design in order to place electric battery, power electronics and electric motors.

To this end, in this paper the attention is focused on P_4 architecture. In this architecture, the few dissipative components between the electric machine and the road allows a highly efficient regeneration of energy as well as lower power consumptions during traction phases. The connection with the ICE, realized through the road [9], allows to completely uncoupling it with the electric motor simply by disengaging the mechanical clutch. Pure electric traction phase is therefore possible.
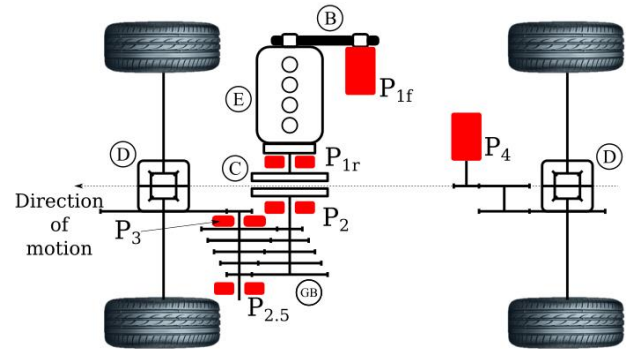

Figure 1. Classification of hybrid architectures based on the position of the secondary energy converter. E = Engine, B = Belt transmission, C = Clutch, GB = Gearbox, D = Differential.

Furthermore, when dealing with mild or full hybrid architectures it is expected that the regenerative braking is the functionality with the highest influence on the overall fuel consumption reduction and efficiency improvement. The motivation is demonstrated by the fact that recovering a consistent amount of energy on-board allows other functionalities to take place (e.g. electric traction, engine assist, and engine boost) for no additional cost. Of crucial interest for the designer is therefore the knowledge of the optimal battery size able to meet constraints of added mass, recoverable energy and dischargeable power.

The subject of the battery sizing for hybrid electric vehicles has already been covered in the literature, and the different methodologies can be subdivided as a function of the typology of hybrid vehicles they are applied to.

1.1 Battery sizing for Hybrid Electric Vehicles.

In early works of Rahman et al. [13, 14] the battery capacity selection is discussed and it is defined with the goal of satisfying the electric motor's peak power. In [10], different hybrid vehicle architectures are analyzed with the goal of finding optimal configuration and size of the energy storage system. The main design variables involve vehicle mass, volume, cost and efficiency, varied as a function of the configurations by means of scaling coefficients and summed to form an objective function to be minimized. Different types of energy storages including a flywheel, a compressed air storage, a Ni-MH battery and ultra-capacitors are taken into consideration. Dynamic programming technique is applied in [15] to overcome the influence of the control strategy. Scaling factors are applied to ICE, electric motor and battery

power to analyze different rates of hybridization while full and torque split hybrid configurations are considered. The results show lower hybridization requirements for full hybrid with respect to torque split configuration. Optimal sizing methodology for torque split mild hybrid powertrain components is studied in [16], where dynamic programming is compared to a simple rule-based so called Equilibrium Point Strategy (EPS). In the rule-based methodology, the hybridization ratio of powertrain is defined to have an equilibrium between regenerative braking energy and required electric traction energy. The results show that optimal hybridization ratios obtained through the global optimization are very close to the ones obtained by means of EPS.

Anselma et.al [17] demonstrates the Power split HEV component sizing using so called slope-weighted energy-based rapid control analysis (SERCA). However, the battery sizing issue is not directly discussed.

Summarizing the methods of sizing the HEV battery present in the literature, it can be highlighted that the battery capacity is derived from the maximum traction power of the electric motor (i.e. maximum allowed discharge current of the battery) as:

$$Q_{kWh} = \frac{P_{em.max}}{C_{max} \cdot \eta_{b.dchg}} \tag{1}$$

or

$$Q_{Ah} = \frac{P_{em.max}}{V \cdot C_{max} \cdot \eta_{b.dchg}} \tag{2}$$

where Q_{kWh} and Q_{Ah} - battery capacity in kWh or Ah, $P_{em.max}$ - maximum power of the electric motor, V - battery nominal voltage, C_{max} - maximum discharge rate of the battery, $\eta_{b.dchg}$ - average discharge efficiency of the battery.

1.2 Battery sizing for Plug-in Hybrid Electric Vehicles.

The possibility to extend a hybrid electric vehicle to a plug-in hybrid by adding an external battery to an existing one is studied in [18]. Based on different rules and assumptions implemented in the energy management strategy of the vehicle, an optimal size of the additional battery is obtained. NiMH technology is found to be the best compromise between vehicle performance and battery cost and volume. Markel and Simpson [19] present a method for the electric battery sizing based on full electric driving range, while in [20], convex optimization is applied to minimize objective functions composed by operational and HEV components' costs.

The battery capacity degrades with the life [21, 22, 23, 24], which is referred as battery ageing [21] and can be estimated with battery state of health [22].

In [23] and [24], the battery size of PHEV is defined considering its ageing by introducing a degradation factor.

Synthesizing methods of PHEV battery sizing methodologies, the Equation (3) can be used without considering the battery degradation:

$$Q_{kWh} = \frac{\Delta E_{max}}{\Delta SOC} \tag{3}$$

Where ΔE_{max} maximum energy required for driving in full electric range (kWh) and ΔSOC is the battery SOC variation during the electric range.

The analysis of the relevant literature about battery sizing of hybridized powertrains highlighted that the particular attention is paid to the use of a charge sustaining control strategies. They can be categorized as rule- or optimization-based strategies. In the rule-based strategies, ICE either provides a constant torque or works at Optimal Operating Line. The electric motor assists the ICE by adding or absorbing the extra torque. In the optimization-based strategies, different optimization techniques are used to define the torque split that minimizes the objective function with the goal of fuel consumption reduction. However, all these strategies utilize the charging of the battery by using ICE during the motion. This can lead to a battery size different from one needed to be enough for storing only the recovered braking energy.

1.3 Contribution of the Paper.

Based on the above analysis, what seems to be missing in the literature is a detailed analysis that focuses on how to size the battery of a mild parallel hybrid vehicle able to recover all the braking energy considering a motion on different driving cycles. In this regard, the use of a charge depleting strategy is reasonable since it maximizes the utilization of regenerated energy, while allowing recovering further energy in successive braking phases. Furthermore, it is of interest to understand what could be the maximum electric traction speed, which can guarantee the complete utilization of the regenerated energy allowing the equilibrium between the recovered and the utilized electrical energy. The main operational unknowns such as the driving cycle itself or the initial state of charge of the battery are also accounted in a large sensitivity analysis that has the goal to highlight, already in a design phase, how to select the proper battery size for the kind of vehicles under analysis.

This paper presents a battery sizing methodology applied to a P4 Mild HEV configuration. In this architecture, the few dissipative components between the electric machine and the road allows a highly efficient regeneration of energy as well as low power consumptions during traction phases. The connection with the ICE, realized through the road, allows to completely uncoupling it with the electric motor by simply disengaging the mechanical clutch. Pure electric traction phase is therefore also allowed. In the proposed methodology, first, the maximum amount of recoverable energy over different driving cycles is analytically computed to establish a reference value, obtainable in the absence of any kind of powertrain losses. This value provides a first input to the battery sizing in case of complete and perfect regeneration. Considering a simple torque split strategy, the vehicle runs in pure electric mode up to a certain vehicle speed (electric traction speed) allowed by the e-powertrain limitations, while the

remaining speed range is run in ICE-mode. Provided to guarantee the equilibrium between recovered and used energy, the fuel consumption can be compared for different battery sizes. A more refined design method is finally presented, including the effects of the maximum electric traction speed, the initial battery state of charge and its capacity.

The main contribution of the paper, therefore, is the development of a method for sizing the battery of a P4 mild HEV architecture able to achieve compromise between recovered energy and its utilization for different driving cycles while avoiding battery oversizing. The proposed methodology considers main constraints coming from powertrain, battery as well as electric motor traction capability.

2. HYBRID ELECTRIC VEHICLE MODELING

A forward modeling approach [2, 4, 25] for the hybrid electric vehicle has been selected due to its ability to reproduce the physical causality of the system while generating the typical driver commands (e.g. throttle, braking commands). The general structure of the model is shown in Figure 2. The model implementation of the main powertrain components (Longitudinal motion logic, ICE, P$_4$ electric motor, battery) will be highlighted. Furthermore, the energy management strategy will be described in detail. The vehicle and powertrain main specifications are given in Table 1.
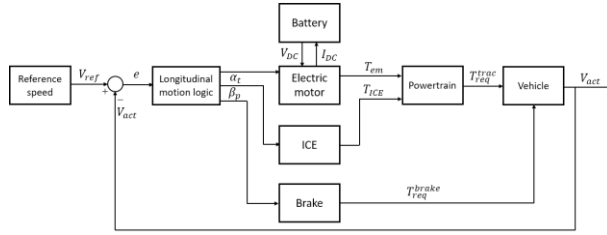

Figure 2. Forward model implementation.

2.1 Longitudinal motion logic

The Longitudinal motion logic block computes the required throttle position (α_t) and braking pressure (β_p) using a PI controller. The input to the PI controller is the difference (speed error) e between reference vehicle speed V_{ref} and actual speed of the vehicle V_{act}.

$$\left(\alpha_t, \beta_p\right) = K_P\left(V_{act} - V_{ref}\right) + K_I \int_0^T \left(V_{act} - V_{ref}\right)dt$$
(4)

with:

$$\begin{cases} 0 \leq \alpha_t \leq 100 & e \geq 0 \ (Traction) \\ 0 \leq \beta_p \leq p_{max} & e < 0 \ (Braking) \end{cases}$$

where T is the simulation time, K_P and K_I are the proportional and integral controller gains and p_{max} is the maximum brake hydraulic circuit pressure.

Furthermore, the block generates the gearshift signal based on the crankshaft angular speed. The upper limit of the crankshaft speed to perform an upshift is 2500 rpm and the lower limit to downshift is 1100 rpm. The process of the shifting the gear is utilized with a hysteresis loop to avoid frequent and unnecessary gear shifting.

Parameter	Value
Vehicle	
Weight	1700 kg
Tire	215/55 R17
Aerodynamic drag coefficient	0.35
Frontal area	2.43 m^2
Engine	
Type	1.4 l, gasoline engine
Maximum power	100 kW
Maximum torque	230 Nm
6 speed manual gearbox	
Gear ratios	4.2, 2.3, 1.4, 0.98, 0.76, 0.6
Final drive ratio	4.44
Electric motor	
Peak power	30 kW
Peak torque	90 Nm
Li-Ion Battery cell	
Nominal voltage	3.6 V
Nominal capacity	4.4 Ah

Table 1. Vehicle and powertrain data
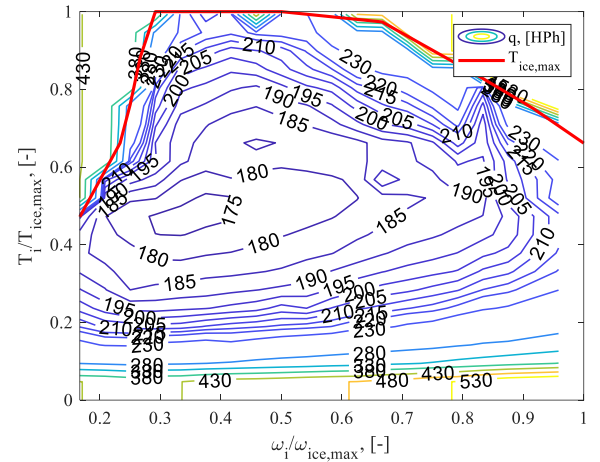
2.2 Internal Combustion Engine

Figure 3. Internal combustion engine specific fuel consumption (q [g/HPh]) contour lines as a function of engine torque and rotational speed (both are represented as the ratio to max. value) and WOT characteristics.

The ICE is modeled based on static maps. Mechanical torque T_{ice} is computed by means of the throttle aperture α_{ice} defined by the controllers and through the torque-speed map (Figure 3) defining the maximum engine torque ($T_{ice,max}$) in wide open throttle (WOT) conditions as a function of the rotational speed of the engine itself (ω_{ice}):

$$T_{ice} = \alpha_{ice} \, T_{ice,max}(\omega_{ice})$$
(5)

Fuel mass flow rate $\dot{m}_{fuel}$ is computed based on the mechanical power P_{ice} produced by the ICE and the specific fuel consumption q, as:

$$\dot{m}_{fuel} = P_{ice} \, q \tag{6}$$

Fuel mass is obtained by integrating the mass flow rate over the simulation time. When ICE is in idling conditions (i.e. the mechanical power is zero) the fuel consumption is set to a constant value.

The net torque at the output from the ICE crankshaft is therefore:

$$T_{ice}^{out} = T_{ice} - J_{ice}\dot{\omega}_{ice} \tag{7}$$

Where, J_{ice} is the crankshaft inertia accounting for flywheel inertia and $\dot{\omega}_{ice}$ is the crankshaft rotational acceleration.

2.3 Electric Motor

The P$_4$ electric motor model was also based on its static torque-speed map, as shown in Figure 4. In addition, the figure provides a map of the absorbed DC currents at the battery level I_{DC} as a function of EM torque (T_{em}) and speed (ω_{em}), and computed as:

$$I_{DC} = (T_{em}\,\omega_{em} + P_{loss})/V_{DC} \tag{8}$$

where V_{DC} is the battery DC link voltage and P_{loss} is the electric machine power loss, accounting for resistive losses only. The motivation for this assumption lies on the fact that copper losses are dominant in the low speed range (where the motor has to work the most) with respect to core losses [2].

The net torque at the electric motor shaft with a moment of inertia J_{em} is:

$$T_{em}^{out} = T_{em} - J_{em}\dot{\omega}_{em} \tag{9}$$

The thermal behavior of the electric motor is modeled by designing its cooling circuit and performance in Motor-CAD environment. The windings temperature θ_{em} dynamics can be described as a first order system:

$$\theta_{em}(t) = K P_{diss}(t)(1 - e^{-t/\tau}) \tag{10}$$

with K and τ defined as the thermal resistance and time constant of the motor. Their interpolated values are implemented in the simulations.

2.4 Battery

The battery pack consists of multiple cells connected in series (to achieve the rated voltage) and parallel (to achieve the desired capacity). The battery pack was modeled as a voltage source V_{oc} in series with a resistance R_b as described in Equation 11.

$$\begin{cases} V_{oc} = N_s V_{oc,cell} \\ R_b = \dfrac{N_s}{N_p} R_{cell} \end{cases} \tag{11}$$

where N_s and N_p are the number of cells connected in series and in parallel, respectively, $V_{oc,cell}$ and R_{cell} are the cell open circuit voltage and resistance.
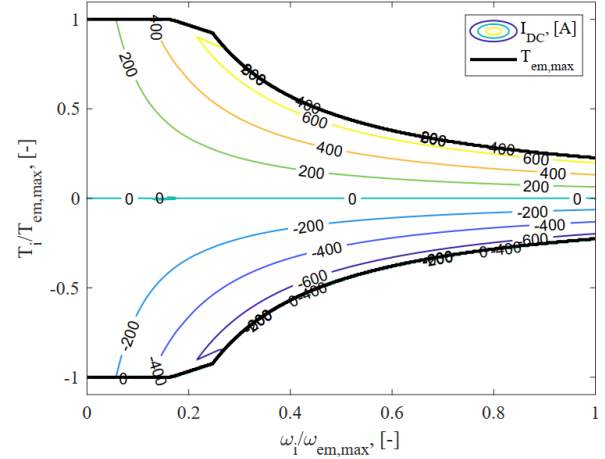

Figure 4. Maximum torque characteristics and DC current map of the electric motor as a function of its torque and speed
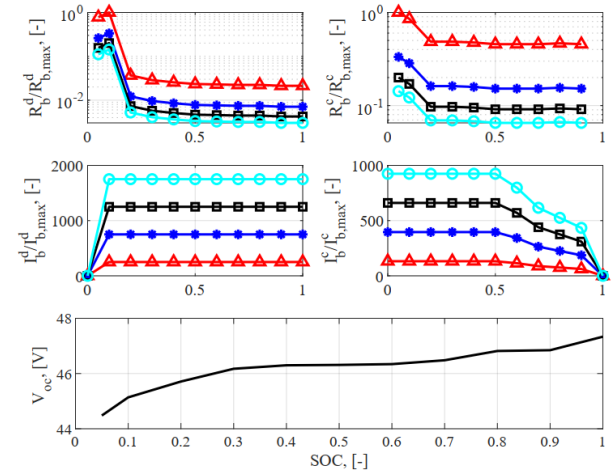

Figure 5. Li-Ion battery characteristics as a function of its SoC. Marked lines are with Q_{nom}: Triangle - 4.4 Ah, Asterisk - 13.2 Ah, Square - 22 Ah, Circle - 30.8 Ah.

The battery state of charge SoC was defined as function of the initial battery state of charge (SoC_0) and of the nominal battery capacity (Q_{nom}) as:

$$SoC = SoC_0 - \int_0^t I_{DC}\,dt \,/Q_{nom} \tag{12}$$

The Figure 5 shows the open circuit voltage, internal resistance and peak DC current (in charge and discharge modes) as function of the state of charge for different capacity values of the considered Li-Ion battery. Charge and discharge modes are evidenced with the superscripts "c" and "d". It should be noticed that the

maximum discharge rate C_{max} is relative high for the considered battery.

2.5 Powertrain

Gearbox and final drive of front and rear powertrain are modeled as transmission ratios with constant efficiencies (equal to 0.96). The torque at the front wheels was:

$$T_w^f = \eta_{gb,f}\eta_{d,f}T_{ice}^{out}\tau_{gb,f}\tau_{d,f} - J_w\dot{\omega}_w \qquad (13)$$

where $\eta_{gb,f}$ and $\eta_{d,f}$ are gearbox and differential efficiencies, $\tau_{gb,f}$ and $\tau_{d,f}$ are gearbox and differential transmission ratios of the front axle, J_w is the wheels inertia and $\dot{\omega}_w$ is the wheels angular acceleration. The torque at the rear wheels was calculated as:

$$T_w^r = \eta_{gb,r}\eta_{d,r}T_{em}^{out}\tau_{gb,r}\tau_{d,r} - J_w\dot{\omega}_w \qquad (14)$$

where $\eta_{gb,r}$ and $\eta_{d,r}$ are gearbox and differential efficiencies, $\tau_{gb,r}$ and $\tau_{d,r}$ are gearbox and differential transmission ratios of the rear axle. The vehicle longitudinal dynamics equation of motion is simply:

$$m\dot{V} = \frac{T_w^f + T_w^r}{R_0} - F_{res} = F_x^f + F_x^r - F_{res} \qquad (15)$$

Where m is the vehicle mass, $\dot{V}$ is the vehicle longitudinal acceleration, R_0 is the tire rolling radius, F_x^f and F_x^r are the front and rear longitudinal forces, and F_{res} is comprehensive of the resistances to motion (aerodynamics, rolling, grade).

2.6 Energy Management System

The energy management system (EMS) is the supervisory controller that continuously interchanges information between the driver requests and the different on-board actuators' control units with the goal of defining the torque set points of engine and electric motor. The EMS is constituted by three main layers described in the following.
The selected control strategy can be considered as a charge depleting action, the simplest strategy that allows complete utilization of the regenerated braking energy and guarantees the energy equilibrium. However, the main difference of the considered control strategy from a conventional charge depleting one is that, either ICE or Electric motor can be used for traction of the vehicle and battery can be recharged only by regenerative braking. The presented method can be then exploited also in the case of the adoption of ICE load shifting as a part of a more sophisticated charge sustaining strategy. This would reflect on different performance in terms of fuel consumption and emissions and consequently on different battery size.

2.6.1 Required Torque Computation.

Based on the maximum capabilities (thermal and electrical) of the powertrain, the required traction torque at the ground level T_{req}^{trac} is computed considering the driver throttle α_t as partialization parameter:

$$T_{req}^{trac} = \alpha_t \cdot \left[T_{ice,max}(\omega)\tau_{gb,f}\tau_{d,f} + T_{em,max}(\omega)\tau_{gb,r}\tau_{d,r}\right] \qquad (16)$$

The required braking torque at the ground level (with mechanical clutch open) is:

$$T_{req}^{brake} = \beta_p \cdot \left[T_{brake} + T_{em,max}(\omega)\tau_{gb,r}\tau_{d,r}\right] \qquad (17)$$

T_{brake} the maximum brake torque realizable by the passive friction brake system. In this case β_p has the goal of partializing the maximum brake torque at the ground level.

2.6.2 Electric Motor and Battery Limitations Computation.

The electric powertrain limitations play a fundamental role on the actual benefits offered by the hybrid architecture. Functional constraints which limit either the electric motor or the battery usage should therefore be evaluated before the required torque computed in previous layer is distributed between front and rear powertrain.
The maximum DC current ($I_{DC,max}$) that can be handled both by the battery and by the electric motor should be firstly computed. Based on the actual battery SoC and on its capacity, the maximum admissible current on the battery side ($I_{DC,max}^b$) is obtained from experimental maps both in charge and in discharge conditions (Figure 5). Similarly, based on the actual electric motor speed, the maximum current manageable by the electric motor ($I_{DC,max}^{em}$) is obtained from maps as shown in Figure 4. Therefore, ($I_{DC,max}$) is obtained based on the following criterion:

$$I_{DC,max} = \min[I_{DC,max}^b(SoC, Q_{nom}), I_{DC,max}^{em}(\omega_{em})] \qquad (18)$$

A inversed version of <u>Figure 4</u> map considering as inputs the actual ω_{em} and the actual $I_{DC,max}$ is used to compute for each time instant the maximum amount of torque that the electric motor can provide to the wheels. This variable is depicted as $T_{em,max}^{nom}$ and was limited based on additional constraints.
By means of rules imposed on the battery SoC and temperature θ_b, and on the electric motor temperature θ_{em} the limitations related to the electric motor traction or braking torques were introduced. Such rules were implemented in this layer using simple membership functions which range between 0 and 1. If any of the limitations do not occur, the functions are all equal to 1, leading the electric motor to be able to realize $T_{em,max}^{nom}$. Even if only one limitation took place, the torque (positive or negative) was then reduced proportionally to the value computed by the membership function, generating a new variable called $T_{em,max}^{lim}$ (positive or

negative). Such variable was the input of the next layer. Furthermore, considering more than one limitations resulted in limiting the product of the different membership functions output. They are set up in order to make the electric powertrain work within its functional ranges:

- Battery charge level: $SoC_{min} < SoC < SoC_{max}$
- Motor temperature: $\theta_{em,min} < \theta_{em} < \theta_{em,max}$
- Battery temperature: $\theta_{b,min} < \theta_b < \theta_{b,max}$

In the simulations, the battery temperature limitation is not enabled, as it requires a development and a validation of more sophisticated electro-thermal modelling. Its introduction can have influence the battery size [30].

As a result, torque limits $T^{lim}_{em,max.Pos}$ and $T^{lim}_{em,max.Neg}$, respectively in traction and braking, are generated. Another limitation not linked with the electric powertrain regards the maximum electric traction vehicle speed. Next section will illustrate the effects that this additional constraint have on the overall energy balance.

2.6.3 Torque Split Strategy.

The torque split strategy controller is responsible for the computation of the correct amount of torque that the different prime movers have to develop in order to let the vehicle follow the prescribed driving cycle. The core functionalities of a mild HEV such as regenerative braking, full electric lunch, Start&Stop were implemented. Therefore, the strategy firstly exploits the maximum capabilities of the electric powertrain, while then use the ICE to drive the vehicle in case the electric powertrain limitations do not allow full electric driving. The torque split factor u is the variable used to determine the torque set points based on the required torque and the electric powertrain limitations. In case of traction ($\alpha_t > 0$) the required torque can be expressed as:

$$T^{trac}_{req} = (1 - u) \cdot T^{act}_{ice} \tau_{gb,f}\tau_{d,f} + u \cdot T^{act}_{em}\ \tau_{gb,r}\tau_{d,r} \quad (19)$$

where T^{act}_{ice} and T^{act}_{em} are the actual torque set points of ICE and electric motor, respectively. The actual torque split strategy was implemented so that:

$$\begin{cases} u = 1 & T^{trac}_{req} < T^{lim}_{em,maxPos}\ \tau_{gb,r}\tau_{d,r} \\ u = 0 & otherwise \end{cases} \quad (20)$$

In such way, if the electric powertrain limitations take place but still allow the motor to produce the required torque, the vehicle is electrically driven only. In all the other cases the ICE only powers the front wheels. Hence, it can be considered as a charge depleting strategy. At each time step, either traction source (ICE or Electric motor) can be used. Charging the battery using the ICE is not considered in the strategy. The hybrid mode (ICE + electric motor) is disabled because the aim is to investigate full potentials of the P4 electric powertrain. This is the main assumption that will be used in the next section regarding the battery sizing.

In case of braking, the required torque was expressed as:

$$T^{brake}_{req} = (1 - u) \cdot T^{act}_b + T^{act}_{em}\ \tau_{gb,r}\tau_{d,r} \quad (21)$$

where T^{act}_b is actual passive brakes torque. Then, the actual torque split strategy was:

$$\begin{cases} u = 1 & T^{brake}_{req} < T^{lim}_{em,maxNeg}\ \tau_{gb,r}\tau_{d,r} \\ u = 0\ \&\ T^{act}_{em} = T^{brake}_{em,maxNeg} & otherwise \end{cases} \quad (22)$$

which means that the priority is given to the electric regenerative braking, and the passive braking is active only to apply the amount of torque not realizable by the electric motor.

A final remark was given regarding the clutch management. To exploit the maximum traction/braking capabilities of P4 architecture, whenever the electric motor was active the clutch disengaged the front powertrain with the rest of the vehicle. In this way, the rear motor has not to overcome the ICE inertia and its over-running torque in traction phases, and some of the available kinetic energy does not dissipate in the ICE during braking.

T^{act}_{ice} and T^{act}_{em} torque set points are therefore sent to their corresponding control units. Thus, the engine control unit generates the correct engine throttle α_{ice} while the inverter sets up the proper current control. However, in this work the modeling of the two aforementioned units is neglected.

3. BATTERY SIZING ANALYSIS

The design of the electric battery for a mild HEV should be focused on the main functionalities of the overall architecture. The regeneration of braking energy owns the highest influence on the fuel economy and, therefore, should be maximized. The use of the electric traction is fundamental to reduce the fuel consumption to avoid the engine to operate at low efficiency regions. Nevertheless, the regeneration and the following use of the energy stored on-board should be balanced in order to optimize the use of the electric powertrain.

In the following, a set of three analysis will be presented, highlighting the role that the different influencing parameters have on the battery size and its energy balance.

3.1 Maximum Recoverable Energy over Cycle

In the first analysis, the amount of energy that can be recovered during a certain driving cycle was computed, assuming neither losses (i.e. 100% efficiency) nor limitations in the powertrain. The stored regenerative energy at the end of each representative cycle is measured.

Using energy modelling, the maximum recoverable energy over a driving cycle is computed as [4, 5, 25]:

$$E_{reg.pot} = E^{trac}_{kin} - \left(E^{brake}_{roll} + E^{brake}_{aero} + E^{brake}_{grade}\right) \quad (23)$$

Figure 6 (top) shows the values of $E_{reg.pot}$ for the different driving cycles analyzed here (NEDC, WLTP, FTP – 75, Artemis). Obviously, the lines connecting the different points have no meaning of data interpolation. They were introduced for a better data visualization only. The amount of recoverable energy was computed both considering a vehicle mass and accounting for the equivalent (apparent) mass due to inertia of rotating components. This increases the recoverable energy due to a higher kinetic energy during the traction phases; however, the increase is in the order of 8-10 %.

Expressing E_{reg} in kJ and considering V_{DC} as a constant value, the recoverable energy in Ah can be computed as:

$$Q_{Ah} = \frac{E_{reg}}{3.6\,V_{DC}} \tag{24}$$

Figure 6 (bottom) shows the effect of the considered driving cycle and of the equivalent inertia on the recoverable energy.

To avoid under-sizing of the battery and, consequently, making it not able to store all the available energy, it is suggested, in a preliminary design phase, to select the driving cycle with highest potential of recoverable energy. In such way, when working on a driving cycle with lower regeneration potential, the total recovery is guaranteed. Although valid only for an initial stage of the design, this analysis leads to an indication of the maximum size of the battery in ideal case.
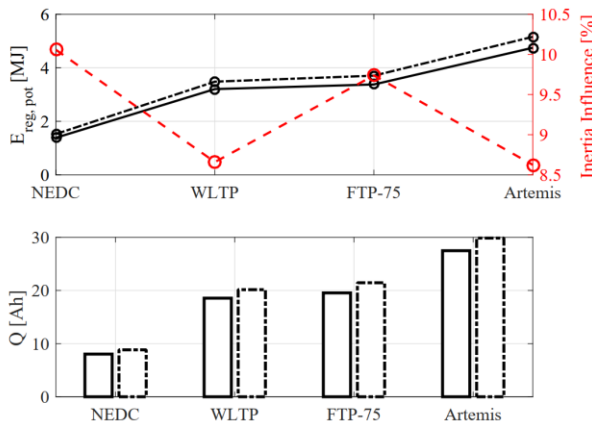

Figure 6. The maximum recoverable energy over different cycles in MJ (top) and converted to Ah (bottom). Solid line – vehicle mass, Dash-doted line – considering equivalent mass of rotating inertias. Dashed line – influence of rotating inertias in %.

3.2 Powertrain Limitations and Battery Capabilities

The second analysis considers both the charge and the discharge phases of the battery, assuming:
- Powertrain efficiency lower than 100%;
- Electric powertrain limitations;
- Reversible battery,

The simulations were performed considering the EMS described in Section 2.6. During traction phases the electric motor torque set point was computed using

Equation 25 (where $T_{req} = T_{req}^{trac}$), until the condition giving $u = 1$ in Equation 20 was satisfied.

$$T_{em}^{act} = \frac{T_{req}}{\tau_{gb,r}\tau_{d,r}} \tag{25}$$

$T_{em,maxPos}^{lim}$ accounts for all the powertrain limitations, including the maximum electric traction vehicle speed. Within this analysis, the latter parameter was set to a very high value so that the vehicle could potentially travel at any speed in pure electric mode. In case of $u = 0$, the required torque is totally provided by the ICE. Similarly, during braking phases electric motor provided the required braking torque ($T_{req} = T_{req}^{brake}$ is used in Equation 25) until the condition $u = 1$ in Equation 21 was valid. Else, blended electric and passive braking torque was used to maximize the regeneration, considering the maximum electric torque capability. Finally, the recovered energy over the driving cycle with the total simulation time T was computed as:

$$E_{reg} = \int_0^T (V_{DC} - R_b^c \cdot |I_{DC}|) \cdot |I_{DC}|\,dt \tag{26}$$

Figure 7 shows the simulations results of total recovered energy E_{reg} as a function of the battery capacity for the four driving cycles under analysis.
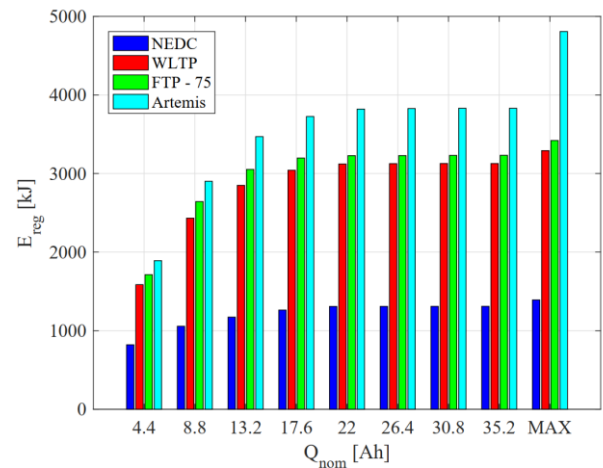

Figure 7. Influence of the battery capacity on the actual recovered energy over different driving cycles. MAX is maximum recoverable energy described in Section 3.1.

The results highlight that the recovered energy increases with increasing battery capacity up to a saturation zone. With increase of battery capacity, higher charge and discharge currents in the battery are allowed, leading to higher recovered energies. Furthermore, the bars labeled with MAX are representative of a maximum recoverable energy in ideal case considered in the analysis in Section 3.1. The difference of recovered energy between 35.2 Ah and MAX capacity is only due to the powertrain efficiencies, introduced in this analysis. The powertrain limitations are not influencing, as the limits are very high.

Due to the saturation of the recovered energy, the minimum battery size able to recover the highest amount of energy while owning the minimum mass can therefore

be found. If the actual recovered energy is translated into a capacity Q_{reg} (Equation 24), when plotting it as a function of the nominal capacity Q_{nom} (Figure 8) in addition to the straight line $Q_{reg} = Q_{nom}$ three main cases can be evidenced:

- $Q_{reg} > Q_{nom}$. The regenerated capacity is higher than the nominal: the battery charges and discharges more than one time each cycle.
- $Q_{reg} = Q_{nom}$. These points lead to a battery size able to store all the recoverable energy while introducing the lowest amount of mass on-board.
- $Q_{reg} < Q_{nom}$. The regenerated energy is lower than the nominal one, that means that the battery is oversized.

Yellow points express the equality between battery capacity and recovered capacity, but since an increase of size would not introduce any consistent increase of the latter, they also represent minimum battery mass points.
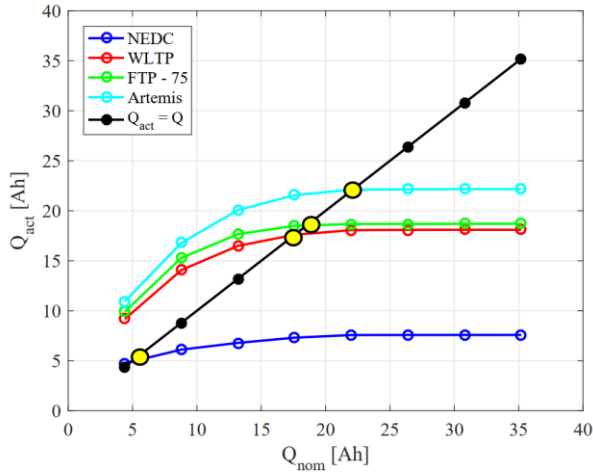

Figure 8. Effect of the battery capacity on the actual recovered energy along different driving cycles.

This analysis has some drawbacks. Since the electric traction is performed without any limitation regarding the consumed energy, the battery continuously works around its minimum state of charge. Although the battery model previously described does not take into account for the state of health [22], it is known from the technology of Li-Ion batteries that similar working conditions lead to consistent damages.

To overcome this issue, next analysis accounts for constraints related to the use of the stored battery energy, introducing the maximum electric traction vehicle speed as a tunable parameter.

3.3 Effect of the Maximum Electric Traction Vehicle Speed and of the Initial State of Charge

In this analysis, the influence of the speed controlled use of the electric traction has on the battery size is pointed out. Since the balance between consumed and recovered energy is a requirement for the sizing, it is clear that the initial state of charge SoC_0 of the battery affects the battery capacity.

The simulations of the previous section were performed setting the electric motor torque reference point to zero whenever the vehicle reached a fixed maximum electric traction vehicle speed. Furthermore, in order to avoid not consistent electric battery working conditions, if the state of charge reaches SoC_{min}, the simulation was stopped and the recovered energy was not evaluated. During the braking phases, the regeneration was not subjected to any constraint.

The profile of the actual and reference speed on a WLTP cycle for a fixed battery capacity of 22 Ah is shown in Figure 9. It shows a good match of two speeds, which indicates the proper selection of PI controller coefficients and the gear shift strategy. Furthermore, the corresponding values of the ICE, the electric motor and the friction brake torques at corresponding wheel level are depicted. It can be seen that in the shown part of the cycle portion the friction brake is not used. The third subplot shows the SOC variation during the portion of the cycle. The initial SOC was 31.5 % in the presented simulation.
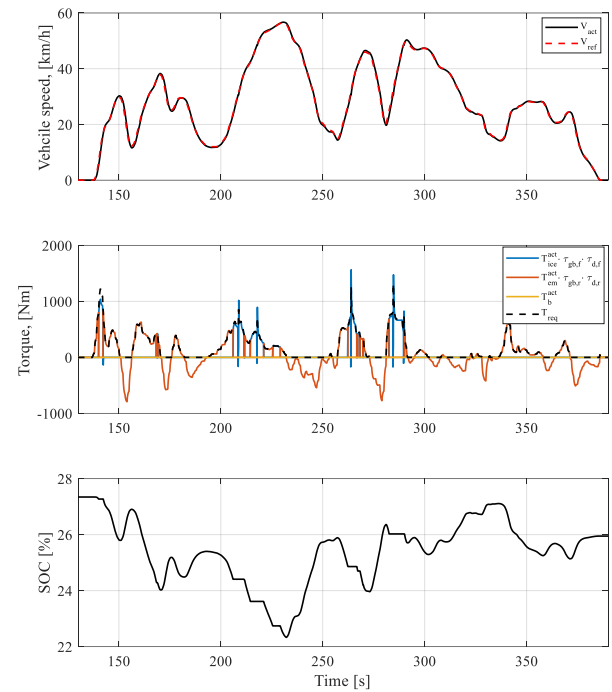

Figure 9. The profile of speeds on portion of WLTP cycle, corresponding torque values at wheel level applied by the ICE, the electric motor and the friction brakes, and SOC time history for configuration with 22 Ah battery capacity. The initial SOC is 31.5 %.

Figure 10 shows the values of recovered energy over a WLTP cycle as a function of different nominal capacities for three different maximum vehicle electric traction speed (20, 30 and 40 km/h). The lower the speed is, the more the regeneration potential reduces due to a limited consumed energy. This is explained by the fact that at low electric traction speeds, the battery cannot discharge enough to recover the braking energy. This phenomenon is amplified by the higher initial state of charge at the beginning of the cycle (continues and dashed lines in Figure 10).

Oppositely, an increase of the consumed energy brought by a higher maximum electric traction vehicle speed leads to a potential energy recovery maximization, as demonstrated by the saturation zone of the Red curves related to $V_{max,PE} = 40$ km/h. In this case, a higher initial state of charge is beneficial because it allows extending the feasible working area to lower battery capacities.
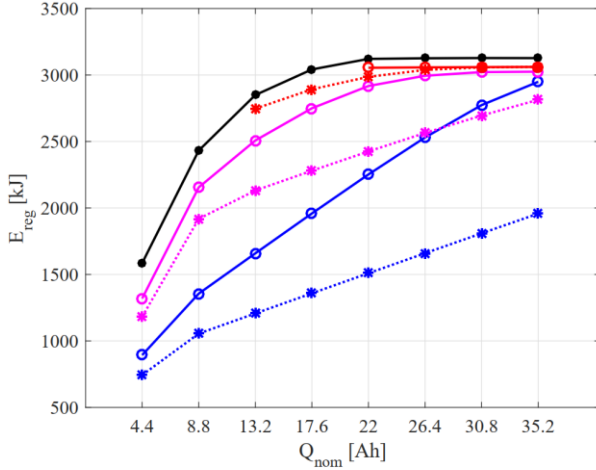

Figure 10. Effect of the battery capacity on the actual recovered energy along WLTP cycle considering different maximum electric traction vehicle speeds and initial state of charge. The maximum vehicle electric traction speed $V_{max,PE}$ is equal to: Blue lines – 20 km/h, Magenta lines – 30 km/h, Red lines – 40 km/h, Black line – energy recovered on WLTP cycle obtained in Section 3.2. Continuous lines: $SoC_0 = 50$ %, dotted lines: $SoC_0 = 70$ %.

The above mentioned fact can be demonstrated in Figure 11 where two values of the battery capacity (4. Ah and 22 Ah) and the initial SOC (50 and 70%) are considered. Figure 11a shows the time history of the battery SOC at 20 km/h electric speed, while Figure 11b is for 40 km/h. The figures highlight that with the smaller battery capacity (the black lines corresponds to 4.4 Ah) the SOC reaches its maximum value faster, due to less utilization of the electric traction. This fact is amplified with low electric traction speed (20 km/h) and higher initial SOC.

It is clear from the presented analysis, that all the mentioned variables (driving cycle, maximum electric traction vehicle speed and initial state of charge) affects the amount of recovered energy, hence they play a central role in the definition of an optimal battery size. This analysis aimed at highlighting the criteria to properly account for them during the design, having clear the goal of energy regeneration maximization and balance between recovered and consumed energy.

The difference between recovered (E_{reg}) and consumed (E_{cons}) energy ΔE is plotted in Figure 12 as a function of the battery size for different maximum electric traction speeds considering a variation in SoC_0 (50 and 70 %) for a WLTP cycle.

$$\Delta E = E_{reg} - E_{cons} \qquad (26)$$

With reference to the lines related to low electric traction speed in Figure 12, ΔE increases with the battery capacity. Since the consumed energy over these lines is the same, the increment is only due to the rise of the effective storable energy, but above a saturation size, ΔE remains constant because the battery is in fully charged condition. In addition, the influence of the initial state of charge is clearly visible. The lower is SoC_0, the smaller is the battery size that allows the charge saturation. A higher SoC_0 moves the battery charge saturation to higher sizes. In such condition, the driving cycle is lunched with an already charged battery, reducing the energy recovery potential.

When the maximum electric traction vehicle speed increases, ΔE reduces due to the increase of the consumed energy. Considering as an example the lines corresponding to a speed of 41 km/h (Red asterisk marker in Figure 12), the initial state of charge affects the achievement of the energetic balance ($\Delta E = 0$): this condition is realized with a smaller battery size when the SoC_0 is high (Figure 12b). This takes place because the battery is already almost fully charged and the energy that can be recovered is exactly equal to that of spent, considering the imposed electric traction speed.

Finally, energy balance points can be found with a certain speed, and they extend to lower battery sizes whenever the initial state of charge is high. It is clear that for equal consumed energy, a battery with lower capacity discharges faster than a battery with higher capacity. If the battery is charged more at the beginning of the driving cycle, even considering a lower capacity, the vehicle is able to follow the prescribed cycle, without reaching the minimum state of charge (SoC_{min}) limitation.

Considering a driving cycle, each of the points present in Figure 12 is named p and is characterized by a capacity, an initial state of charge, a maximum electric traction speed and difference between recovered and consumed energy:

$$p = (Q_{nom}, SoC_0, V_{max,PE}, \Delta E) \qquad (27)$$

The points of equilibrium are points in which the recovered electrical energy equals the consumed electrical energy and are characterized by a value of $\Delta E = 0$. Therefore, assigning the superscript * to such values, it is found that:

$$p^* = (Q_{nom}^*, SoC_0^*, V_{max,PE}^*) \qquad (28)$$

This means that each equilibrium point is characterized by a certain value of battery capacity, initial state of charge and maximum electric traction speed. Thus, focusing on equilibrium points p^* only, it is possible to understand how the battery size and the initial state of charge affects the maximum electric traction speed.

Set of simulations were performed considering a dense range of maximum electric traction speeds, varying SoC_0 between 40 and 70 %. The battery capacity range between 4.4 and 44 Ah was considered.
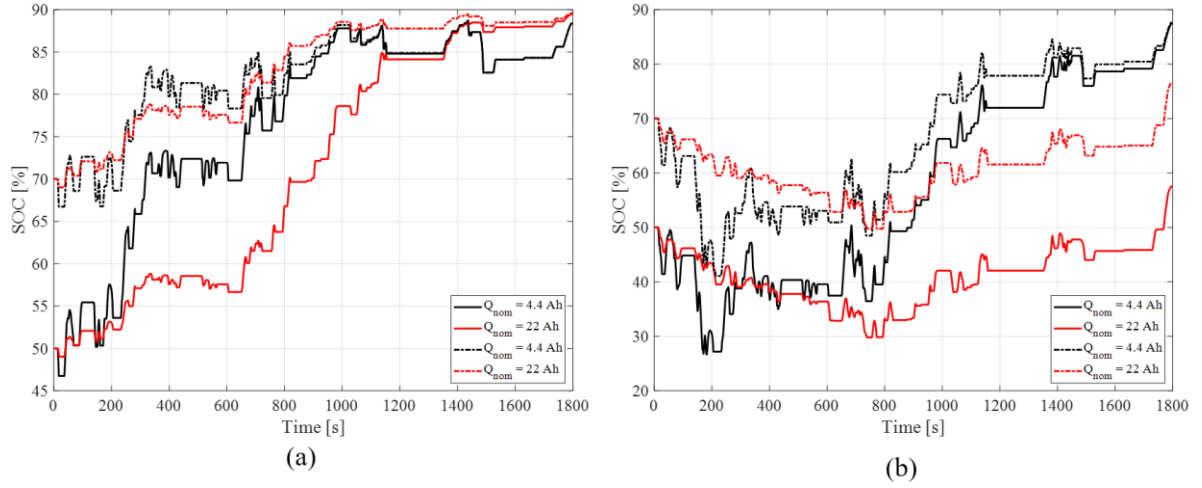
Figure 11. Time history of the battery SOC over WLTP cycle for two different nominal capacity of the battery 4.4 Ah and 22 Ah, SoC_0 = 50 % and 70 % with maximum electric traction speeds (a) 20 km/h and (b) 40 km/h

(a) SoC_0 = 50 %.
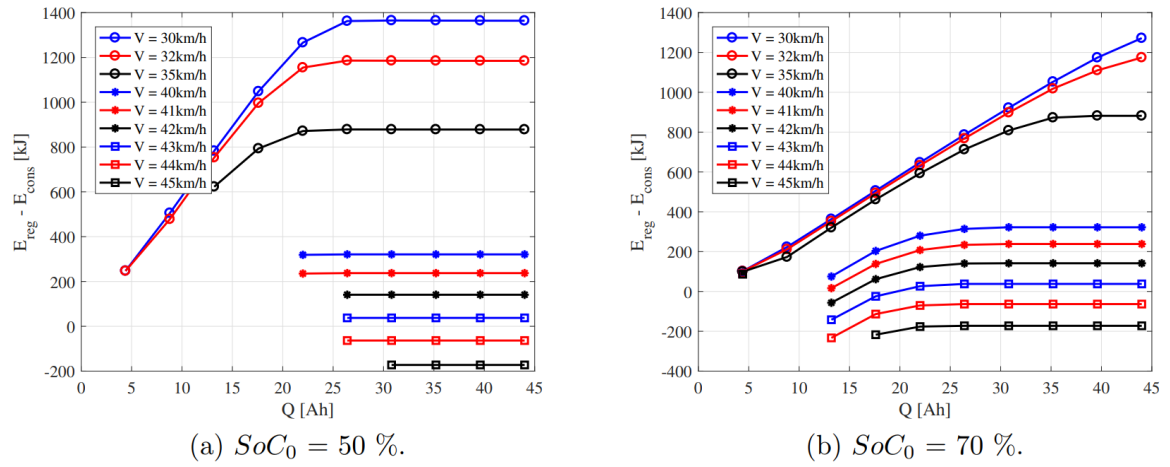
(b) SoC_0 = 70 %.

Figure 12. Difference between recovered and consumed energy over an NEDC cycle as a function of the battery capacity for different maximum electric traction speeds considering (a) SoC_0 = 50 % (a) and (b) SoC_0 = 70 % (b)
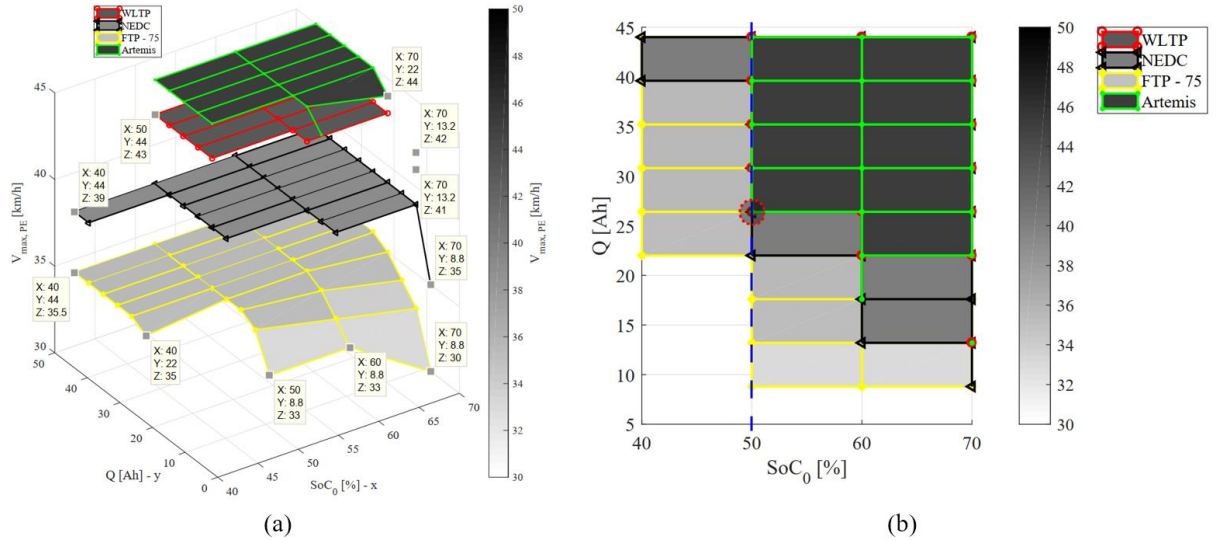

(a)

(b)

Figure 13. (a) Sensitivity analysis regarding the influence of the battery capacity and the initial state of charge on the maximum electric traction vehicle speed that guarantees the energy balance on different driving cycles; (b) Superimposed surfaces and evaluation of minimum admissible battery capacity that ensures the energy balance..

Equilibrium points were obtained for different battery initial state of charge and the vehicle maximum electric traction speed during a certain driving cycle. In this way, the battery size that satisfies the equilibrium conditions was found for different driving cycles.

Figure 13a shows the influence of the battery nominal capacity Q_{nom} and initial state of charge SoC_0 on the vehicle electric traction speed $V_{max,PE}$ which guaranties the energetic equilibrium ($\Delta E = 0$) for different driving cycles under consideration. It should be noted that the equilibrium for that capacity and the initial SOC can be obtained only at certain $V_{max,PE}$.

To obtain the points on surfaces, a certain battery nominal capacity, its initial state of charge and the driving cycle were chosen, while the vehicle electric traction speed was varied to obtain the energetic equilibrium (i.e. the equality of the regenerated and the used electrical energy). The data tips of the points indicate the value of the initial state of charge (X), the nominal battery capacity (Y) and the maximum electric traction vehicle speed (Z) used in the simulation. Once all the possible energy equilibrium points are obtained for the given drive cycle, other drive cycles were used for points generation. The green, red, black and yellow line grid surfaces represent the Artemis, WLTP, NEDC and FTP cycles, respectively. As it can be seen, the surfaces do not cover all the nominal capacity and the initial state of charge points. The motivation behind discarding set of points is that of not being possible to find the electric traction vehicle speed that guarantees the energy equilibrium. Therefore, such points do no present in Figure 13.

With the surfaces obtained in Figure 13a, the battery size selection procedure continues with three more steps, such as:

- Selection of a proper SoC_0;
- Superimposition of the driving cycle surfaces in order to find the minimum battery size admissible for all the cycles;
- Sensitivity analysis on $V_{max,PE}$ in order to evaluate which speed has less impact on the energy balance for all the driving cycles.

The first step is clearly the most difficult to perform. Finding the most representative battery initial state of charge upon which the design should be based is far from being an easy job. The external charging is not provided and it is practically impossible to know it a priori whenever the driver switches on the vehicle after a shutdown. Statistical analysis or experimental tests based on real world driving situations could clearly give better insights regarding this point. For case study only, an intermediate value of $SoC_0 = 50$ % is chosen.

In the second step, the superimposition of the surfaces is performed (Figure 13b). This allows visualizing the area inclusively covered by all the considered drive cycles. The area covered by all the surfaces allows full recovery of the regenerated energy on all the cycles. In such way, the combination of the initial state of charge, the nominal capacity and the maximum electric traction vehicle speed which satisfies the energy equilibrium in various driving conditions can be defined.

By imposing $SoC_0 = 50$ %, the minimum battery capacity able to satisfy the energy balance for all the driving cycles is found to be 26.4 Ah. This battery capacity corresponds to 1.267 kWh capacity considering the nominal battery pack voltage equal to 48 V.

The dotted red point of Figure 13b is characterized by four $V_{max,PE}$, each one optimized for its specific driving cycle. The goal of the last step is to understand which of the four has less impact on its energy balance. A correlation matrix shown in Table 2 can be filled. The speed value $V_{max,PE}$ with the smallest average ΔSoC for different driving cycles (C_n) can be considered as a maximum speed limit.

	$V_{max,PE,1}$	$V_{max,PE,2}$	$V_{max,PE,r}$	$V_{max,PE,n}$
C_1	0	$\Delta SoC_{1,2}$	$\Delta SoC_{1,r}$	$\Delta SoC_{1,n}$
C_2	$\Delta SoC_{2,1}$	0	$\Delta SoC_{2,r}$	$\Delta SoC_{2,n}$
C_3	$\Delta SoC_{3,1}$	$\Delta SoC_{3,2}$	0	$\Delta SoC_{3,n}$
C_4	$\Delta SoC_{4,1}$	$\Delta SoC_{4,2}$	$\Delta SoC_{4,r}$	0

Table 2. A correlation matrix between drive cycle (C_n) and maximum electric traction speed ($V_{max,PE}$) regarding the energy balance.

The analysis described in this section is the most complete one that takes into account the larger number of variables and considers realistic powertrain working conditions. Oppositely, the first analysis takes only into account information of the recoverable energy during the driving cycle and sizing the battery directly based on it. The second analysis, instead, allows obtaining a battery size sufficiently large to maximize the recovered energy, provided that the battery can always work above its minimum admissible charge threshold and assuming a constant initial state of charge of 50 %. If the first analysis leads to an over-dimensioning of the battery capacity, the second one leads to under-dimensioning, while the third lets the designer to consider several driving conditions all together while focusing on real powertrain limitations. Therefore, it can be stated that the third analysis gives an intermediate solution between the first and the second one, considering the simple energy management strategy (pure electric traction – pure thermal traction) while accounting for several realistic driving and working conditions. It can be used as a method for sizing the battery of mild HEVs whenever the full recovery and utilization of braking energy and the electric traction speed are design constraints.

4. CONLUSIONS

This paper presents analysis and methods to size the electric battery for P4 mild HEV. The critical analysis of the existing methods of battery sizing demonstrates that HEV battery are sized either to match maximum power requirement of the electric motor in traction or to be able to deliver enough energy range of electric driving only. However, the sizing with the goal to maximize the regenerative braking energy, so far, is not considered in the literature. Firstly, the energy potential of the different driving cycles is defined. Using forward modelling approach and implementing simple ON-OFF control strategy the sensitivity analysis of how the battery size affects the recovered energy is studied. The influence of the powertrain efficiencies and limitations, initial state of charge of the battery and pure electric traction speed is also highlighted. Finally, the method able to size the battery size that maximizes the benefits due to regeneration of the braking energy is presented.
Future works could involve the battery sizing for different mild HEV architectures with electrified accessories (e.g. electrified water pump, air conditioning compressor, and electrified power steering pump) using different control strategies. The optimization based control strategies that use the load-shifting feature to maximize the fuel economy, obviously requires an additional battery capacity with respect to the minimum size able to recover the available braking energy only. Since, the goal was to address the energy recovery maximization, the use of different control strategies and their influence on the battery size could be scope of another work. It would be also reasonable to investigate the influence of the battery thermal limitations on its size.

REFERENCES

[1] I. E. Agency, "CO2 emissions from fuel combustion. Key trends in CO2 emissions," IEA, 2015.

[2] E. Ali, Advanced electric drive vehicles, CRC Press, 2014, p. 616.

[3] Guardiola, C., B. Pla, S. Onori, and G. Rizzoni, "Insight into the HEV/PHEV optimal control solution based on a new tuning method," *Control Engineering Practice,* vol. 29, pp. 247-256, 2014.

[4] Onori, Simona, Lorenzo Serrao, and Giorgio Rizzoni, Hybrid Electric Vehicles: Energy management strategies, London: Springer, 2016.

[5] Guzzella, Lino, and Antonio Sciarretta, Vehicle propulsion systems, Springer-Verlag Berlin Heidelberg, 2007.

[6] Cheli, Federico, Massimiliano Gobbi, and Nikola Holjevac, "Vehicle subsystems' energy losses and model-based approach for fuel efficiency estimation towards an integrated optimisation," *International Journal of Vehicle Design,* vol. 76, no. 1-4, pp. 46-81, 2018.

[7] Amati, Nicola, Andrea Tonoli, Luca Castellazzi, and Sanjarbek Ruzimov, "Design of electromechanical height adjustable suspension," *Proceedings of the Institution of Mechanical Engineers, Part D: Journal of Automobile Engineering,* vol. 232, no. 9, pp. 1253-1269, 2018.

[8] Melaine Guillou and Calvin Bradley, "Fuel Consumption Testing to Verify the Effect of Tire Rolling Resistance on Fuel Economy," in *SAE Technical Paper*, 2010.

[9] Chen, Ming-Yen, Kang Yang, Yun-Zhong Sun, and Jung-Ho Cheng, "An Energy Management Strategy for Through-the-Road Type Plug-in Hybrid Electric Vehicles," *SAE International Journal of Alternative Powertrains,* vol. 8, no. 1, pp. 61-75, 2019.

[10] Hofman, T., D. Hoekstra, R. M. Van Druten, and M. Steinbuch, "Optimal design of energy storage systems for hybrid vehicle drivetrains," in *IEEE Vehicle Power and Propulsion Conference*, Chicago, IL, 2005.

[11] Di Napoli, Maria, Manuel Strähle, Sanjarbek Ruzimov, LD Suarez Cabrera, Nicola Amati, and Andrea Tonoli, "Intelligent belt drive systems in hybrid powertrains: a multipurpose test rig," in *IFAC-PapersOnLine 49, no. 21 (2016): 47-53.*, 2016.

[12] "eMobility is our future.," MAGNA, [Online]. Available: http://electrification.magna.com/powertrain-electrification/. [Accessed 15 May 2020].

[13] Rahman Ziaur, Karen L. Butler, and Mehrdad Ehsani, "A study of design issues on electrically peaking hybrid electric vehicle for diverse urban driving patterns," in *SAE Technical Paper 1999-01-1151*, 1999.

[14] Rahman, Ziaur, Karen L. Butler, and Mehrdad Ehsani, "A comparison study between two parallel hybrid control concepts," in *SAE Technical Paper 2000-01-0994*, 2000.

[15] Sundström, Olle, Lino Guzzella, and Patrik Soltic, "Optimal hybridization in two parallel hybrid electric vehicles using dynamic programming," in *IFAC Proceedings Volumes*, 2008.

[16] Sundstrom, Olle, Lino Guzzella, and Patrik Soltic, "Torque-assist hybrid electric powertrain sizing: From optimal control towards a sizing law," *IEEE Transactions on Control Systems Technology,* vol. 18, no. 4, pp. 837-849, 2009.

[17] Pier Giuseppe Anselma, Atriya Biswas, Lucas Bruck, Saeed Amirfarhangi Bonab, Adam Lempert, Joel Roeleveld, Krishna Madireddy, Omkar Rane, Bryon Wasacz, Giovanni Belingardi, Ali Emadi, «Accelerated Sizing of a Power Split Electrified Powertrain,» in *WCX SAE World Congress Experience, SAE Technical Paper 2020-01-0843*, 2020.

[18] Tara, Ehsan, Soheil Shahidinejad, Shaahin Filizadeh, and Eric Bibeau, "Battery storage sizing in a retrofitted plug-in hybrid electric vehicle," *IEEE Transactions on Vehicular Technology,* vol. 59, no. 6, pp. 2786-2794, 2010.

[19] Markel, Tony, and Andrew Simpson, "Plug-in hybrid electric vehicle energy storage system design," Golden, CO (United States), 2006.

[20] Pourabdollah, Mitra, Nikolce Murgovski, Anders Grauers, and Bo Egardt, "Optimal sizing of a parallel PHEV powertrain," *IEEE Transactions on Vehicular Technology,* vol. 62, no. 6, pp. 2469-2480, 2013.

[21] Liu, Zifan, Simona Onori, and Andrej Ivanco, "Synthesis and experimental validation of battery aging test profiles based on real-world duty cycles for 48-V mild hybrid vehicles," *IEEE Transactions on Vehicular Technology ,* vol. 66, no. 10, pp. 8702-8709, 2017.

[22] Bonfitto, Angelo, Ethelbert Ezemobi, Nicola Amati, Stefano Feraco, Andrea Tonoli, and Shailesh Hegde, "State of Health Estimation of Lithium Batteries for Automotive Applications with Artificial Neural Networks," in *AEIT International Conference of Electrical and Electronic Technologies for Automotive (AEIT AUTOMOTIVE)*, 2019.

[23] Murgovski, Nikolce, Lars Mårdh Johannesson, and Bo Egardt, "Optimal battery dimensioning and control of a CVT PHEV powertrain," *IEEE Transactions on Vehicular Technology,* vol. 63, no. 5, pp. 2151-2161, 2013.

[24] Song, Ziyou, Xiaobin Zhang, Jianqiu Li, Heath Hofmann, Minggao Ouyang, and Jiuyu Du, "Component sizing optimization of plug-in hybrid electric vehicles with the hybrid energy storage system," *Energy,* vol. 144, pp. 393-403, 2018.

[25] Mukhitdinov, A. A., S. K. Ruzimov, and S. L. Eshkabilov, "Optimal control strategies for CVT of the HEV during a regenerative process," in *IEEE Conference on Electric and Hybrid Vehicles*, Pune, India, 2006.

[26] Huang Yanjun, Hong Wang, Amir Khajepour, Bin Li, Jie Ji, Kegang Zhao, and Chuan Hu, "A review of power management strategies and component sizing methods for hybrid vehicles," *Renewable and Sustainable Energy Reviews,* vol. 96, pp. 132-144, 2018.

[27] Faris, Waleed F., Hesham A. Rakha, Raed Ismail Kafafy, Moumen Idres, and Salah Elmoselhy, "Vehicle fuel consumption and emission modelling: an in-depth literature review," *International Journal of Vehicle Systems Modelling and Testing ,* vol. 6, no. 3-4, pp. 318-395, 2011.

[28] Sundstrom, Olle, and Anna Stefanopoulou, "Optimal power split in fuel cell hybrid electric vehicle with different battery sizes, drive cycles, and objectives," in *IEEE International Conference on Control Applications*, 2006.

[29] Sundström, Olle and Stefanopoulou, Anna, "Optimum Battery Size for Fuel Cell Hybrid Electric Vehicle— Part I," *Journal of Fuel Cell Science and Technology,* vol. 4, no. 2, pp. 167-175, 2006.

[30] Samad, Nassim A., Youngki Kim, and Jason B. Siegel. "On power denials and lost energy opportunities in downsizing battery packs in hybrid electric vehicles." *Journal of Energy Storage,* 16 (2018): 187-196.